Chemistry–A European Journal
Full Paper
doi.org/10.1002/chem.202102630
Chemistry Europe
European Chemical Societies Publishing
www.chemeurj.org

Special Collection

A Semiconductor-Mediator-Catalyst Artificial Photosynthetic System for Photoelectrochemical Water Oxidation

Fujun Niu[+],[a, b] Degao Wang[+],[b, c] Lenzi J. Williams,[b] Animesh Nayak,[b] Fei Li,[b] Xiangyan Chen,[a] Ludovic Troian-Gautier,[b] Qing Huang,[c] Yanming Liu,[b] M. Kyle Brennaman,[b] John M. Papanikolas,[b] Liejin Guo,[a] Shaohua Shen,*[a] and Thomas J. Meyer*[b]

Abstract: In fabricating an artificial photosynthesis (AP) electrode for water oxidation, we have devised a semiconductor-mediator-catalyst structure that mimics photosystem II (PSII). It is based on a surface layer of vertically grown nanorods of Fe_2O_3 on fluorine doped tin oxide (FTO) electrodes with a carbazole mediator base and a Ru(II) carbene complex on a nanolayer of TiO_2 as a water oxidation co-catalyst. The resulting hybrid assembly, **FTO|Fe_2O_3|–carbazole|TiO_2|–Ru(carbene)**, demonstrates an enhanced photoelectrochemical (PEC) water oxidation performance compared to an electrode without the added carbaozle base with an increase in photocurrent density of 2.2-fold at 0.95 V vs. NHE and a negatively shifted onset potential of 500 mV. The enhanced PEC performance is attributable to carbazole mediator accelerated interfacial hole transfer from Fe_2O_3 to the Ru(II) carbene co-catalyst, with an improved effective surface area for the water oxidation reaction and reduced charge transfer resistance.

Introduction

Research on artificial photosynthesis (AP) focused on photoelectrochemical (PEC) water splitting is attracting increasing attention.[1,2] The four electron overall reaction for converting water into O_2, with its associated complexities, is critical in the design of cells for artificial photosynthesis.[3,4] In 1972, Fujishima and Honda reported that bandgap excitation of TiO_2 in the UV for water oxidation.[5] In their experiments, TiO_2 was both the light absorber and, following injection, the catalyst for water oxidation. In natural photosynthesis at PSII, absorbed light is transferred to the P680 chromophore where oxidative equivalents are transferred to the Mn_4CaO_5 catalyst cluster through a tyrosine electron transfer mediator for O_2 production.[6–9]

Compared with organic chromophores, semiconductors are promising for their high stability, low-cost synthesis, accessibility for large-scale applications, and for good light response in the visible region.[10–12] Among the available semiconductors, hematite (α-Fe_2O_3) with a band gap of 1.9 to 2.2 eV, has been widely used for PEC water oxidation because it is an excellent visible light absorber with high stability in alkaline solutions and has earth-abundant sources.[13] However, use of hematite as a light absorber in the oxygen evolution reaction (OER), results in photocurrents that are well below limiting values because of charge recombination in both the bulk oxide and on surfaces. Performance is decreased significantly in neutral and acidic solutions because of unfavorable kinetics for the OER.[13]

To enhance hematite PEC water oxidation performance, research has been pursued based on morphological engineering, doping, and the use of heterojunctions.[13,14] Of interest here is surface modification by added molecular co-catalysts with matching redox potentials that occur in hybrid photoanodes.[13,15,16] The latter combine the advantages of Fe_2O_3 light harvesting, with broad visible light response and good stability under oxidative conditions, and molecular catalysis with facile linkage to electrodes and flexible redox properties. This approach has the advantage of extracting photo-generated holes from the surface of Fe_2O_3 with internal transfer from the oxide to an external molecular unit. One value of an increase in the distance between light harvester and catalytic center is the inhibition of back electron transfer to the electrode. In these assemblies, "charge carrier/molecular complex" ratios are large

[a] Dr. F. Niu,[+] Dr. X. Chen, Prof. L. Guo, Prof. S. Shen
International Research Center for Renewable Energy (IRCRE)
State Key Laboratory of Multiphase Flow in Power Engineering (MFPE)
Xi'an Jiaotong University (XJTU),
28 West Xianning Road, Xi'an, Shaanxi 710049 (P. R. China)
E-mail: shshen_xjtu@mail.xjtu.edu.cn

[b] Dr. F. Niu,[+] Dr. D. Wang,[+] Dr. L. J. Williams, Dr. A. Nayak, Prof. F. Li, Dr. L. Troian-Gautier, Prof. Y. Liu, Dr. M. K. Brennaman, Prof. J. M. Papanikolas, Prof. T. J. Meyer
Department of Chemistry
University of North Carolina at Chapel Hill
Chapel Hill, North Carolina 27599 (United States)
E-mail: tjmeyer@unc.edu

[c] Dr. D. Wang,[+] Prof. Q. Huang
Engineering Laboratory of Advanced Energy Materials
Ningbo Institute of Industrial Technology, Chinese Academy of Sciences
Ningbo, Zhejiang, 315201 (P. R. China)

[+] These authors contributed equally to this work.

Supporting information for this article is available on the WWW under https://doi.org/10.1002/chem.202102630

Special Collection This manuscript is part of a special collection dedicated to Vincenzo Balzani on the occasion of his 85th birthday.

and may benefit the generation of catalytic intermediates in appropriate redox states for water oxidation.[17]

Electron transfer to external catalysts has also been investigated[18–24] with recognition of the role that tyrosine plays in the activation of the P680 chromophore toward electron transfer from the Mn_4CaO_5 catalyst in PSII. The mediator increases the lifetime of redox equivalents by avoiding back electron transfer from the Mn_4CaO_5 catalyst to oxidized P680.[9] In photocatalytic systems a variety of mediators have been explored including methyl viologen,[18] carbon nanofibers,[20] graphene oxide[21] and TiO_2,[22] and other oxides. In dye sensitized photoelectrosynthesis cells (DSPEC), the mediator undergoes rapid and efficient charge transfer from Ru(II) polypyridyl complexes such as $[Ru(4,4\text{-}(PO_3H_2)_2\text{-}2,2\text{-bipyridine})(2,2\text{-bipyridine})_2]^{2+}$[23] and a benzimidazole-phenol[24]. However, there are limited examples of molecular mediators in this area with reduced graphene oxide[25] and TiO_2[26] commonly used. As far as we know, hematite-mediator-catalyst based PEC photoanode has never been reported.

In the current work, we synthesized the carbazole, 9-(4-(dihydroxyphosphonato)phenyl)]-3,6-di-tert-butyl-9H-carbazole, as a mimic for the tyrosine residue in PSII. In a final assembly for water oxidation on the surface of Fe_2O_3, we combined the carbazole with the water oxidation carbene co-catalyst, $[Ru^{II}(tpy\text{-}Ph\text{–}CH_2\text{–}PO_3H_2)(Mebim\text{-}py)(H_2O)](PF_6)_2$ (tpy-Ph–CH_2–PO_3H_2 = (4-([2,2′:6′,2″-terpyridin]-4′-yl)benzyl) phosphonic acid; Mebim-py = 3-methyl-1-pyridyl-benzimidazol-2-ylidene), on a nanoparticle layer of TiO_2 (Figure 1a). The resulting **FTO|Fe_2O_3|–carbazole|TiO_2|–Ru(carbene)** hybrid photoanode undergoes photoelectrochemical (PEC) water oxidation with photocurrents that increase from 40 to 90 μA/cm^2 at 0.95 V vs. NHE and with a 500 mV negative shift in onset potential compared to **FTO|Fe_2O_3|TiO_2|–Ru(carbene)**. Enhanced performance with the added base arises from promoted hole transfer from the Fe_2O_3 anode to the Ru(carbene) catalyst because of the increase in distance between the oxide electrode and the catalyst with the added carbazole mediator.

Experimental Methods

Detailed experimental methods are available in the Supporting Information.

Results and Discussion

Photoanode

The structure of the hybrid photoanode with α-Fe_2O_3 as the light absorber, the carbazole base as the mediator, and a Ru(II) polypyridyl carbene complex as the catalyst, is shown in Figure 1a. **FTO|Fe_2O_3** films, composed of vertically grown nanorods on FTO coated glass with thicknesses > 600 nm and a diameter of ~50 nm (see Figure S3 in Supporting Information,†), were prepared by using published procedures (see details in Experimental Procedures).[27] A synthetic procedure describing the characterization of the carbazole base is given in the Supporting Information †. In a first step in preparing the anode assembly, **FTO|Fe_2O_3** was soaked in a methanol/acetonitrile (v:v = 1:3) solution containing 1 mM carbazole for 6 h for attachment. Surface coverage by the base of 1.2 nmol/cm^2 was evaluated by UV-vis absorption measurements (see Characterization in Experimental Procedures for details). The **FTO|Fe_2O_3|–carbazole** slides that resulted, were washed with a methanol/acetonitrile solution to remove the excess carbazole. Following addition of the base, a thin layer of TiO_2 (~0.8 nm) was added by atomic layer deposition (ALD). Addition of the TiO_2 layer provided an external metal oxide support for binding the Ru(carbene) catalyst. The latter was synthesized by a previously reported procedure.[28] After deposition of the TiO_2 film, the **FTO|Fe_2O_3|–carbazole|TiO_2** electrode was rinsed in a methanol solution with 2 mM Ru(carbene) catalyst to give the final electrode, **FTO|Fe_2O_3|–carbazole|TiO_2|–Ru(carbene)**. Spectrophotometric analysis of the electrode showed that the final surface coverage of the carbene catalyst was 0.9 nmol/cm^2. The relatively small surface coverages both the carbazole and Ru(carbene) catalyst probably be attributed to the large nanorod morphology of the **FTO|Fe_2O_3** electrodes and their relatively small surface areas.

The results of cyclic voltammetry (CV) measurements on the carbazole and Ru(carbene) co-catalyst on *nano*ITO electrodes in 0.5 M Na_2SO_4 solutions at pH 4.7 are shown in Figure S4. In CVs of the Ru(carbene) co-catalyst, oxidation waves appear at 1 V and 1.3 V vs. NHE for the $Ru^{III/II}$ and $Ru^{IV/III}$ catalyst couples. Further oxidation past Ru(IV) to Ru(V) was obscured by the background electrode oxidation past ~1.5 V.[29,30] In solutions containing the carbazole, an irreversible oxidation also appears ca. 1.7 V vs. NHE at a potential more positive than the onset

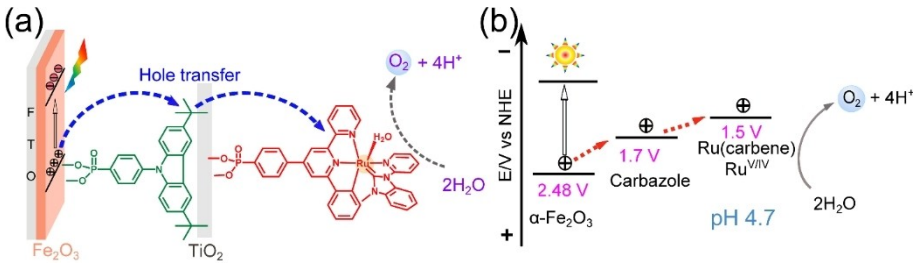

Figure 1. (a) Structure of **FTO|Fe_2O_3|–carbaozle|TiO_2|–Ru(carbene)** assemblies illustrating surface electron transfer. (b) A corresponding energy level diagram for water oxidation in pH 4.7 Na_2SO_4 with visible light irradiation.

potential for the $Ru^{V/IV}$(carbene) catalyst wave at $Ru^{V/IV}$ ~1.5 V vs. NHE. The valence band (VB) potential for hematite occurs at 2.48 V vs. NHE,[31] and as shown in Figure 1b, photo-generated holes are thermodynamically capable of undergoing hole transfer from the VB of Fe_2O_3 to the carbazole molecule, and, further, to the Ru(carbene) co-catalyst to induce water oxidation following visible light irradiation.

Photoelectrocatalysis

The PEC behavior of the **FTO|Fe_2O_3|–Carbazole|TiO_2|–Ru-(carbene)** hybrid electrode was monitored by current-potential measurements (Figure 2a and S3a), and chronoamperometry (Figure 2b and S3b) with irradiation >400 nm. Standard three electrode cells used with working electrodes to monitor water oxidation under 1 Sun illumination (100 mW/cm^2, 400 nm cut-off filter). A platinum mesh electrode was used as the counter electrode for water reduction with a Ag/AgCl (3 M KCl) reference electrode.

Based on the data in Figures 2a and 2b, apparent water oxidation by **FTO|Fe_2O_3** under the same conditions occurs with a photocurrent density of only 15 μA/cm^2 at 0.95 V vs. NHE (1.23 V vs. RHE) and with a large onset potential, ~1.2 V vs. NHE. The electrode is ineffective toward water oxidation because of recombination both in the bulk and on the surface.[13] Attaching the Ru-(carbene) catalyst to the TiO_2 binding layer to give **FTO|Fe_2O_3|–carbazole|TiO_2|–Ru(carbene)**, caused a negative shift in onset potential of ~400 mV and an increase in photocurrent from 15 to 40 μA/cm^2 (see Figure 2a and 2b) relative to **FTO|Fe_2O_3**. Considering that both TiO_2 and the Ru(carbene) catalyst could improve PEC performance compared to **FTO|Fe_2O_3** (see Figure S5), the enhancement for **FTO|Fe_2O_3|–carbazole|TiO_2|–Ru(carbene**) may has its origin in a "defects quenching" effect as the TiO_2 layer is formed[32–34] or by enhanced water oxidation kinetics for the Ru(carbene) catalyst.[29,30] When the carbazole mediator was added between Fe_2O_3 and the Ru(carbene) molecule, as shown in Figure 2a and 2b, the resulting **FTO|Fe_2O_3|–carbazole|TiO_2|–Ru(carbene)** electrode shows improved PEC performance with an onset potential negatively shifted for 500 mV and photocurrent increased by 2.2-fold compared to the **FTO|Fe_2O_3|TiO_2|–Ru(carbene) electrode**. The mechanism of the reaction, and a related discussion are presented below.

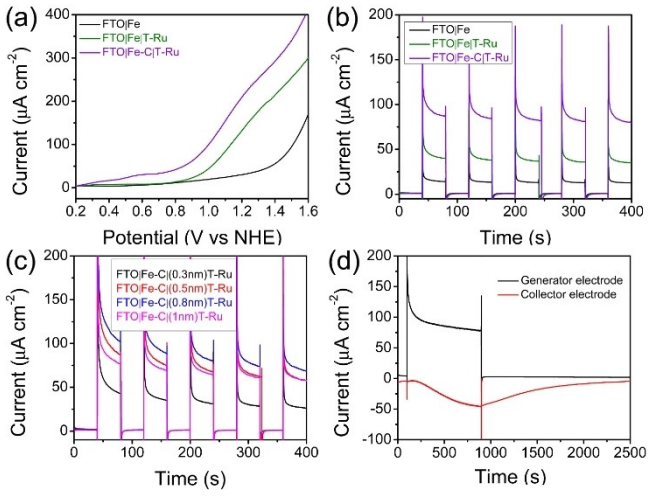

Figure 2. (a) Current-potential curves, (b) current-time traces, and (c) current-time response for the electrodes, **FTO|Fe_2O_3|–carbazole|(x)TiO_2|–Ru-(carbene)**, with different thickness of TiO_2. (d) O_2 measurements for water oxidation (black) from **FTO|Fe_2O_3|–carbazole|TiO_2|–Ru(carbene)** with visible irradiation (100 mW/cm^2, 400 nm cut-off filter) from 60 to 900 s at a bias of 0.95 V vs. NHE in 0.5 M Na_2SO_4 (pH 4.7) solution. The applied bias for the current-time traces was 0.95 V vs. NHE. The red current-time response was for an O_2 collector electrode held 1 mm from the photoanode poised at −0.65 V vs. NHE. The thickness of TiO_2 in (a) and (b) is 0.5 nm. In the diagrams the abbreviations for Fe_2O_3, carbazole, TiO_2 and Ru(carbene) were Fe, C, T and Ru. The same abbreviations are used in other Figures in the text.

The role of the thickness of the TiO_2 layer in the electrodes **FTO|Fe_2O_3|–carbazole|(x)TiO_2|–Ru(carbene)** was also investigated. In the calculations, the calculated length of carbazole was taken to be 1 nm. As shown in Figure 2c, an assembly with a TiO_2 thickness of 0.3 nm gave a relatively low photocurrent of ca. 50 μA/cm^2 at an applied potential of 0.95 V vs. NHE. The low value is probably due to inefficient coverage by carbazole on the TiO_2 overlayer and with it, inhibited attachment of the Ru(carbene) co-catalyst. As the thickness of the TiO_2 layer was increased, coverage by carbazole led to enhanced attachment by the catalyst. At a thickness of 0.8 nm, the assembly reached its point of highest photocurrent density, ~90 μA/cm^2. With a further increase to 1 nm, the photocurrent fell from 90 to 75 μA/cm^2 at 0.95 V vs. NHE perhaps because the total coverage of the carbazole hindered hole transfer from the carbazole mediator to the Ru(carbene) catalyst. Given the positive effect of TiO_2 on the performance of **FTO|Fe_2O_3**, the dependence of the thickness of the TiO_2 on the **FTO|Fe_2O_3** core was also investigated. As shown in Figure S6, the optimized thickness of TiO_2 deposited on **FTO|Fe_2O_3** was 0.5 nm, different from the optimized 0.8 nm thickness in the electrode, **FTO|Fe_2O_3|–carbazole|(x)TiO_2|–Ru(carbene)**. This result suggests that a TiO_2 thickness dependence on the performance of **FTO|Fe_2O_3|–carbazole|(x)TiO_2|–Ru(carbene)** could be related to hole transfer from carbazole to Ru(carbene)catalyst rather than from the well-known surface modification of **FTO|–Fe_2O_3** by TiO_2.[32–34]

To test the efficiency and stability of **FTO|Fe_2O_3|–carbazole|(0.8 nm)TiO_2|–Ru(carbene)** toward water oxidation, collector-generator (C-G) experiments were conducted with an in situ analysis of O_2 by using a procedure described elsewhere.[35–37] In a typical experiment, O_2 evolved at the photoanode diffuses over a controlled distance to a second collector electrode for O_2 analysis. At the end of a photolysis cycle, O_2 was evaluated to the second electrode with the Faradic efficiency (FE) for water oxidation evaluated by current measurements, equation 1, with $Q_{collector}$ and $Q_{generator}$ representing charges passed at the collector and generator electrodes. The constant 0.7 is the collection efficiency for the collector electrode.[37]

$$\frac{\frac{Q_{collector}}{Q_{generator}}}{0.7} \times 100\,\% = FE(\%) \quad (1)$$

As shown in Figure 2d and Figure S7, during 14 min photolysis cycles, only slight decreases in O_2 photocurrent were observed possibly from corrosion of hematite in acidic conditions. Compared to the bare **FTO**|–**Fe_2O_3** electrode, the **FTO**|**Fe_2O_3**|**(0.8 nm)TiO_2**|–**Ru(carbene)** assembly results in FE values from 78% to 90%. With the addition of carbazole in **FTO**|**Fe_2O_3**|–**carbazole**|**(1 nm)TiO_2**|–**Ru(carbene)**, the FE reached an impressive 94% for O_2 evolution. The latter is probably due to the enhanced interface hole transfer induced by TiO_2 and the carbazole mediator and the fast OER by Ru(carbene) catalyst.

The decreases in photocurrent for **FTO**|**Fe_2O_3** and **FTO**|**Fe_2O_3**|–**carbazole**|**(0.8 nm)TiO_2**|–**Ru(carbene)** suggest that both carbazole and the Ru(carbene) co-catalyst remain surface bound over the 14 min photolysis period. XPS was used to ascertain the chemical composition of the **FTO**|**Fe_2O_3**|–**carbazole**|**(0.8 nm)TiO_2**|–**Ru(carbene)** surface before and after photolysis. Following PEC water oxidation measurements over 14 min, the ratios of Ru/P/N in **FTO**|**Fe_2O_3**|–**carbazole**|**(0.8 nm)TiO_2**|–**Ru(carbene)** was 1:1.9:6.2, consistent to the expected value of 1:2:6 in the assembly. Similar comparison for the Ru 2p resonance for the **FTO**|**Fe_2O_3**|–**carbazole**|**(0.8 nm)TiO_2**|–**Ru(carbene)** before and after photolysis (see Figure S8), also shows that there were no chemical shifts for the Ru 2p resonances, indicating that the Ru(carbene) unit also remains attached over the 14 min PEC water oxidation cycles.

Incident photon to current efficiencies (IPCE) for **FTO**|**Fe_2O_3**, **FTO**|**Fe_2O_3**|**(0.8 nm)TiO_2**|–**Ru(carbene)**, and **FTO**|**Fe_2O_3**|–**carbazole**|**(0.8 nm)TiO_2**|–**Ru(carbene)** were evaluated in 0.5 M Na_2SO_4 solution (pH 4.7). The data were analyzed by using equation 2 with I the photocurrent density, λ the incident light wavelength (nm) and J_{light} the power density of the monochromatic light at a specific wavelength.

$$IPCE = \frac{(1240I)}{(\lambda J_{light})} \quad (2)$$

As shown in Figure S9a and Figure S1d, as expected, the IPCE profiles overlap well with the spectral distribution of light adsorption by Fe_2O_3. The IPCE for **FTO**|**Fe_2O_3** is 0.37% at 450 nm. With introduction of the Ru(carbene) co-catalyst on the thin layer of TiO_2, the IPCE was increased from 0.37% to 1.39% at 450 nm presumably due to an enhanced local charge density and reduced recombination with the added Ru(carbene) co-catalyst. Further addition of carbazole in **FTO**|**Fe_2O_3**|–**carbazole**|**(0.8 nm)TiO_2**|–**Ru(carbene)**, increased the IPCE to 2% at 450 nm compared to 1.39% in **FTO**|**Fe_2O_3**|**(0.8 nm)TiO_2**|–**Ru(carbene)** supporting an important role for carbazole in the final assembly.

The role of added carbazole was further explored by luminescence measurements on **FTO**|**Fe_2O_3 and FTO**|**Fe_2O_3**|–**carbazole**. Following excitation of light at 450 nm in air, as shown in Figure S9b, a broad photoluminescence (PL) emission centered at 650 nm was observed from a band-edge transition with a red shift of ~50 nm due to a Stokes shift.[38,39] Upon attaching with carbazole molecule, the emission of **FTO**|**Fe_2O_3** was quenched, indicating there is no passivation effect of carbazole on the surface of **FTO**|**Fe_2O_3**.[40,41] This decrease in PL emission intensity suggests the suppressed charge recombination of Fe_2O_3, which should be ascribed to the possible hole transfer from Fe_2O_3 to the attached carbazole molecule.[22,42,43]

Electrochemistry

The role of the carbazole in the assemblies was further investigated by electrochemical measurements in the dark (see Figure 3 and in Figures S8 and S9). Linear sweep voltammograms (LSV) were obtained in 0.5 M Na_2SO_4 solutions at pH 4.7. As shown in Figure S10a, with the addition of carbazole, electrochemical water oxidation by **FTO**|**Fe_2O_3** was greatly enhanced with a positively shifted onset potential and higher current density consistent with the PEC results in Figure 2a.

The role of the added base on band bending behavior at the semiconductor/electrolyte interface was also investigated by Mott-Schottky (M-S) analysis in the same medium.[43,44] As shown in Figure S10b, the flat band potential for **FTO**|**Fe_2O_3** is maintained at 0.22 V vs. NHE even after the addition of the carbazole with no evidence for a role by carbazole on band bending. The electrochemical double-layer capacitance (C_{dl}) between the anode and electrolyte, used for evaluating the effective contact area, was recorded by CV (Figure S11) with results shown in Figure 3a.[20] Addition of the carbazole molecule induced an increased C_{dl} for **FTO**|**Fe_2O_3** from 26.7 to 36.8 μF/cm^2 consistent with an enhanced effective electro-

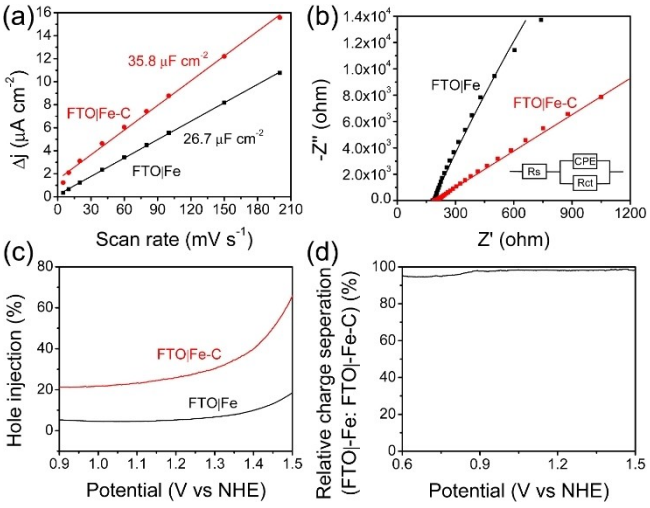

Figure 3. (a) Current density variation (△j) as a function of scan rate at an overpotential of 0.56 V vs. NHE to estimate the effective electrochemical areas of **FTO**|**Fe_2O_3** and **FTO**|**Fe_2O_3**|–**carbazole** electrodes. (b) EIS Nyquist plots measured at 0.95 V vs. NHE with the fitted equivalent electrical circuit diagrams (inset) of **FTO**|**Fe_2O_3** and **FTO**|**Fe_2O_3**|–**carbazole** electrodes. (c) Interface hole injection efficiencies for **FTO**|**Fe_2O_3** and **FTO**|**Fe_2O_3**|–**carbazole** photoelectrodes for water oxidation. (d) The relative charge separations in **FTO**|**Fe_2O_3** and **FTO**|**Fe_2O_3**|–**carbazole** electrodes in 0.5 M Na_2SO_4 solutions with H_2O_2 (0.1 M) added as a hole scavenger.

chemical area for the electrode. The latter is in agreement with the PEC and LSV results in Figures 2a and S8a.

The interface charge transfer resistance (R_{ct}) between **FTO|Fe_2O_3** and the electrolyte was investigated by electrochemical impedance spectroscopy (EIS). The Nyquist plots that were obtained from the analysis are shown in the inset of Figure 3b, where the semicircle is attributable to interfacial charge transfer, R_s is the series resistance, CPE is the capacitance associated with Helmholtz layer at the electrode/solution interface, and R_{ct} is the interfacial charge transfer resistance.[20] From the data, it is obvious that R_{ct} in **FTO|Fe_2O_3** was decreased with added carbazole which enhances charge transfer kinetics at the interface. The electrochemical observations are all consistent with electron transfer rate enhancements with added carbazole.

Hole injection efficiency

As shown in equation 3, the water oxidation photocurrent (J) is a product of the photon absorption rate (J_{abs}), the photo-generated charge separation yield ($P_{separation}$), and the hole injection yield ($P_{injection}$). In these experiments we adopted a method used elsewhere with H_2O_2 as a sacrificial reagent to capture photo-generated holes on the surface of **FTO|Fe_2O_3**.[45,46] When H_2O_2 was added as a hole scavenger to the electrolyte, the observed current was the product of J_{abs} and $P_{separation}$ because $P_{injection}$ is 100% in equation 4, with the hole injection efficiency as the ratio of photocurrents with and without added H_2O_2 (see Figure S12). Based on the data in Figure 3c, the hole injection efficiency for **FTO|Fe_2O_3** was increased from 4.8% to 21% at 0.95 V vs. NHE after addition of carbazole. The approximate 100% bulk charge separation efficiency of **FTO|Fe_2O_3** to **FTO|Fe_2O_3|–carbazole** in Figure 3d indicates that carbazole couldn't have an influence on the bulk charge transfer of Fe_2O_3. Based on the electrochemical and steady state PL results, there is an improved hole injection efficiency for the **FTO|Fe_2O_3|–carbazole** hybrid electrode compared to **FTO|Fe_2O_3**, which presumably arises from a decreased interface charge transfer resistance and higher effective electrochemical area.

$$J_{H_2O} = J_{abs} \times P_{separation} \times P_{injection} \quad (3)$$

$$J_{H_2O_2} = J_{abs} \times P_{separation} \quad (4)$$

Transient Absorption

The microscopic dynamics of the electrodes was investigated by ultrafast transient absorption measurements with a 470 nm pulsed excitation source. Data in Figure S13 show time-resolved spectra for the **FTO|Fe_2O_3** and **FTO|Fe_2O_3|–carbazole** under a 1 V applied electrical bias (1.47 V vs. RHE) in 0.5 M Na_2SO_4 solution (pH 4.7). The spectral features observed in the TA spectra for the two are similar with an initial broad, positive absorption feature at 600 nm which extends to ~800 nm. The transient absorption features observed following visible excitation arise from the appearance of transient intermediates. The appearance of the negative bleach signal at ~575 nm for hematite under positive bias arises from electron trapping localized states close to the conduction band edge.[46] The transient signal at >625 nm is a hematite hole absorption. In the transient spectrum, the spectral inversion occurs at wavelengths expected for photo-induced holes at the surface of the hematite.[46]

Transient kinetics were evaluated at both 575 nm and 750 nm. The time dependences at both wavelengths could be accurately represented by tri-exponential kinetics. It is evident from the data in Figure S14 that the dynamics at 575 nm for **FTO|Fe_2O_3** and **FTO|Fe_2O_3|–carbazole** are similar arising from a transient with a lifetime of 460 ps do to electron decay within **FTO|Fe_2O_3**. Photo-generated hole kinetics at 750 nm were distinct for the two in Figure 4. Adding carbazole to the assembly decreased the bleach amplitude compared to **FTO|Fe_2O_3**. The decay of holes at the **FTO|Fe_2O_3** surface were characterized by tri-exponential kinetics with the lifetimes and amplitudes: τ_1 (ps) = 5.50 ± 2.84 (7%), τ_2 (ps) = 487 ± 128 (59%), and a long-lived component >1 ns (34%). Trapped hole based kinetics at **FTO|Fe_2O_3|–carbazole** occurred with the amplitude lifetimes: 0.34 ± 0.02 (27%), 171 ± 52 (11%), and a long-lived lifetime >1 ns (62%). Analysis of the kinetics data also showed that carbazole decreased the hole half-life for **FTO|Fe_2O_3** from 520 to 210 ps with a role for carbazole in promoting hole transfer.

Based on the short time scale data, the carbazole base plays a major role. In PSII in nature, a tyrosine residue serves as the mediator between the Mn_4CaO_5 catalyst and the P680 light harvester for efficient charge transfer.[6–9] In the modified electrode, **FTO|Fe_2O_3|–carbazole|(0.8 nm)TiO_2|–Ru(carbene)**, carbazole acts as the hole transfer mediator promoting hole transfer from Fe_2O_3 to the Ru(carbene) co-catalyst for water oxidation.

Conclusion

We have reported here a hybrid semiconductor-mediator-catalyst photoelectrochemical (PEC) cell that mimics the PSII in natural photosynthesis for water oxidation but based on Fe_2O_3

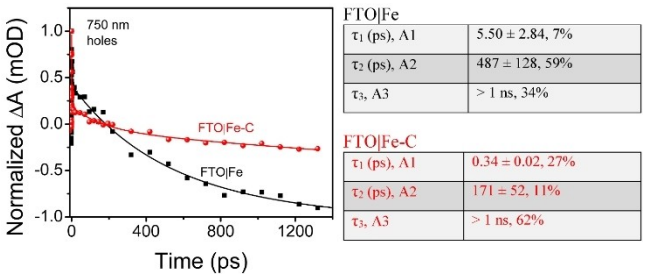

FTO|Fe	
τ_1 (ps), A1	5.50 ± 2.84, 7%
τ_2 (ps), A2	487 ± 128, 59%
τ_3, A3	> 1 ns, 34%

FTO|Fe-C	
τ_1 (ps), A1	0.34 ± 0.02, 27%
τ_2 (ps), A2	171 ± 52, 11%
τ_3, A3	> 1 ns, 62%

Figure 4. Single-wavelength TA traces at 750 nm of **FTO|Fe_2O_3** and **FTO|Fe_2O_3|–carbazole** electrodes with corresponding lifetimes.

as a chromophore oxide support with added carbazole as a redox mediator base, and a Ru(carbene) water oxidation catalyst added by attachment through a TiO_2 binding layer. The final **FTO|Fe_2O_3|–carbazole|(0.8 nm)TiO_2|–Ru(carbene)** electrode behaved as a water oxidation photoanode toward water oxidation to O_2 with a 2.2-fold photocurrent enhancement and 500 mV negative shift of onset potential compared to **FTO|Fe_2O_3|(0.8 nm)TiO_2|–Ru(carbene)** as the photoelectrode. The added carbazole base leads to a significant enhancement in PEC performance by promoting interfacial hole transfer from the Fe_2O_3 photosensitizer to the Ru(carbene) catalyst. carbazole acts as an electron transfer mediator similar to the tyrosine residue in PSII. Addition of carbazole decreases the lifetimes of photo-generated holes from 520 to 210 ps. These results demonstrate a novel semiconductor-mediator-catalyst artificial photosynthesis (AP) system with a bioinspired organic mediator for efficient water oxidation.

Supporting Information

Supporting Information contains characterizations of the carbazole, α-Fe_2O_3, added experimental data, X-ray photoelectron spectroscopic data and the results of ultrafast transient absorption (TA) experiments.

Funding Information

This research was primarily supported by the Alliance for Molecular PhotoElectrode Design for Solar Fuels (AMPED), an Energy Frontier Research Center (EFRC) funded by the U.S. Department of Energy, Office of Science, Office of Basic Energy Sciences, under Award No. DE-SC0001011. X-ray photoelectron spectroscopy and ALD experiments were performed at the Chapel Hill Analytical and Nanofabrication Laboratory, CHANL, a member of the North Carolina Research Triangle Nanotechnology Network, RTNN, which is supported by the National Science Foundation, Grant ECCS-1542015. The synthesis of Fe_2O_3 was supported by the Basic Science Center Program for Ordered Energy Conversion of the National Natural Science Foundation of China (No. 51888103) (X.C., S.S. and L. G.).

Acknowledgements

The authors thank Dr. C. Donley at CHANL for assistance with X-ray photoelectron spectroscopy analysis. F.N. thank the support from the China Scholarship Council.

Conflict of Interest

The authors declare no conflict of interest.

Keywords: heterogeneous catalysis · photocatalysis · photoelectrochemistry water oxidation · water splitting

[1] B. Shan, M. K. Brennaman, L. Troian-Gautier, Y. Liu, A. Nayak, C. M. Klug, T. Li, R. M. Bullock, T. J. Meyer, *J. Am. Chem. Soc.* **2019**, *141*, 10390–10398.
[2] F. Niu, D. Wang, F. Li, Y. Liu, S. Shen, T. J. Meyer, *Adv. Energy Mater.* **2019**, 1900399.
[3] J. D. Blakemore, R. H. Crabtree, G. W. Brudvig, *Chem. Rev.* **2015**, *115*, 12974–13005.
[4] D. Wang, R. N. Sampaio, L. Troian-Gautier, S. L. Marquard, B. H. Farnum, B. D. Sherman, M. V. Sheridan, C. J. Dares, G. J. Meyer, T. J. Meyer, *J. Am. Chem. Soc.* **2019**, *141*, 7926–7933.
[5] A. Fujishima, K. Honda, *Nature* **1972**, *238*, 37.
[6] Y. Umena, K. Kawakami, J. Shen, N. Kamiya, *Nature* **2011**, *473*, 55–60.
[7] N. Cox, D. A. Pantazis, F. Neese, W. Lubitz, *Acc. Chem. Res.* **2013**, *46*, 1588–1596.
[8] T. Irebo, M. Zhang, T. F. Markle, A. M. Scott, L. Hammarström, *J. Am. Chem. Soc.* **2012**, *134*, 16247–16254.
[9] M. Wang, K. Han, S. Zhang, L. Sun, *Coord. Chem. Rev.* **2015**, *287*, 1–14.
[10] S. Hennessey, P. Farràs, *Chem. Commun.* **2018**, *54*, 6662–6680.
[11] F. Li, H. Yang, W. Li, L. Sun, *Joule* **2018**, *2*, 36–60.
[12] M. Wang, Y. Yang, J. Shen, J. Jianga, L. Sun, *Sustain. Energy Fuels* **2017**, *1*, 1641–1663.
[13] S. Shen, S. A. Lindley, X. Chen, J. Z. Zhang, *Energy Environ. Sci.* **2016**, *9*, 2744–2775.
[14] RK. Sivula, F. Le Formal, M. Grätzel, *ChemSusChem* **2011**, *4*, 432–449.
[15] S. M. Lauinger, B. D. Piercy, W. Li, Q. Yin, D. L. Collins-Wildman, E. N. Glass, M. D. Losego, D. Wang, Y. V. Geletii, C. L. Hill, *ACS Appl. Mater. Interfaces* **2017**, *9*, 35048–35056.
[16] L. Wu, A. Nayak, J. Shao, T. J. Meyer, *Proc. Natl. Acad. Sci. USA* **2019**, *116*, 11153–11158.
[17] H. Chen, S. Ardo, *Nat. Chem.* **2017**, *10*, 17–23.
[18] H. Lu, R. Hu, H. Bai, H. Chen, F. Lv, L. Liu, S. Wang, H. Tian, *ACS Appl. Mater. Interfaces* **2017**, *9*, 10355–10359.
[19] W. T. Eckenhoff, R. Eisenberg, *Dalton Trans.* **2012**, *41*, 13004–13021.
[20] F. Niu, C. Dong, C. Zhu, Y. Huang, M. Wang, J. Maier, Y. Yu, S. Shen, *J. Catal.* **2017**, *352*, 35–41.
[21] H. Kasap, R. Godin, C. Jeay-Bizot, D. S. Achilleos, X. Fang, J. R. Durrant, E. Reisner, *ACS Catal.* **2018**, *8*, 6914–6926.
[22] F. Niu, S. Shen, L. Guo, *J. Catal.* **2016**, *344*, 141–147.
[23] D. Wang, M. S. Eberhart, M. V. Sheridan, K. Hu, B. D. Sherman, A. Nayak, Y. Wang, S. L. Marquard, C. J. Dares, T. J. Meyer, *Proc. Natl. Acad. Sci. USA* **2018**, *115*, 8523–8528.
[24] Y. Zhao, J. R. Swierk, J. D. Megiatto, B. Sherman, W. J. Youngblood, D. Qin, D. M. Lentz, A. L. Moore, T. A. Moore, D. Gust, T. E. Mallouk, *Proc. Natl. Acad. Sci. USA* **2012**, *109*, 15612–15616.
[25] S. Ye, C. Ding, R. Chen, F. Fan, P. Fu, H. Yin, X. Wang, Z. Wang, P. Du, C. Li, *J. Am. Chem. Soc.* **2018**, *140*, 3250–3256.
[26] J. J. Leung, J. Warnan, D. H. Nam, J. Z. Zhang, J. Willkomm, E. Reisner, *Chem. Sci.* **2017**, *8*, 5172–5180.
[27] Y. Fu, C. Dong, Z. Zhou, W. Lee, J. Chen, P. Guo, L. Zhao, S. Shen, *Phys. Chem. Chem. Phys.* **2016**, *18*, 3846–3853.
[28] Y. Wang, S. L. Marquard, D. Wang, C. Dares, T. J. Meyer, *ACS Energy Lett.* **2017**, *2*, 1395–1399.
[29] M. R. Norris, J. J. Concepcion, Z. Fang, J. L. Templeton, T. J. Meyer, *Angew. Chem. Int. Ed.* **2013**, *52*, 13580–13583; *Angew. Chem.* **2013**, *125*, 13825.
[30] M. R. Norris, J. J. Concepcion, D. P. Harrison, R. A. Binstead, D. L. Ashford, Z. Fang, J. L. Templeton, T. J. Meyer, *J. Am. Chem. Soc.* **2013**, *135*, 2080–2084.
[31] Y. Xu, M. Schoonen, *Am. Mineral.* **2000**, *85*, 543–556.
[32] X. Yang, R. Liu, C. Du, P. Dai, Z. Zheng, D. Wang, *ACS Appl. Mater. Interfaces* **2014**, *6*, 12005–12011.
[33] D. Barreca, G. Carraro, A. Gasparotto, C. Maccato, M. E. A. Warwick, K. Kaunisto, C. Sada, S. Turner, Y. Gönüllü, T. Ruoko, L. Borgese, E. Bontempi, G. Van Tendeloo, H. Lemmetyinen, S. Mathur, *Adv. Mater. Interfaces* **2015**, *2*, 1500313.
[34] M. G. Ahmed, I. E. Kretschmer, T. A. Kandiel, A. Y. Ahmed, F. A. Rashwan, D. W. Bahnemann, *ACS Appl. Mater. Interfaces* **2015**, *7*, 24053–24062.
[35] D. Wang, M. V. Sheridan, B. Shan, B. H. Farnum, S. L. Marquard, B. D. Sherman, M. S. Eberhart, A. Nayak, C. J. Dares, A. K. Das, R. M. Bullock, T. J. Meyer, *J. Am. Chem. Soc.* **2017**, *139*, 14518–14525.

[36] D. Wang, S. L. Marquard, L. Troian-Gautier, M. V. Sheridan, B. D. Sherman, Y. Wang, M. S. Eberhart, B. H. Farnum, C. J. Dares, T. J. Meyer, *J. Am. Chem. Soc.* **2018**, *140*, 719–726.
[37] B. D. Sherman, M. V. Sheridan, C. J. Dares, T. J. Meyer, *Anal. Chem.* **2016**, *88*, 7076–7082.
[38] S. Shen, C. X. Kronawitter, J. Jiang, S. S. Mao, L. Guo, *Nano Res.* **2012**, *5*, 327–336.
[39] L. Xu, J. Xia, L. Wang, J. Qian, H. Li, K. Wang, K. Sun, M. He, *Chem. Eur. J.* **2014**, *20*, 2244–2253.
[40] D. Cao, W. Luo, J. Feng, X. Zhao, Z. Li, Z. Zou, *Energy Environ. Sci.* **2014**, *7*, 752–759.
[41] J. Wang, J. Yang, Z. Zheng, T. Lu, W. Gao, *Appl. Catal. B* **2017**, *218*, 277–286.
[42] F. Wen, X. Wang, L. Huang, G. Ma, J. Yang, C. Li, *ChemSusChem* **2012**, *5*, 849–853.
[43] F. Niu, S. Shen, N. Zhang, J. Chen, L. Guo, *Appl. Catal. B* **2016**, *199*, 134–141.
[44] F. Niu, S. Shen, J. Wang, L. Guo, *Electrochim. Acta* **2016**, *212*, 905–911.
[45] T. Hisatomi, H. Dotan, M. Stefik, K. Sivula, A. Rothschild, M. Grätzel, N. Mathews, *Adv. Mater.* **2012**, *24*, 2699–2702.
[46] S. R. Pendlebury, X. Wang, F. Le Formal, M. Cornuz, A. Kafizas, S. D. Tilley, M. Grätzel, J. R. Durrant, *J. Am. Chem. Soc.* **2014**, *136*, 9854–9857.

Manuscript received: August 27, 2021
Version of record online: February 3, 2022